Showcasing research from Professor Kumagai's laboratory, Graduate School of Pharmaceutical Sciences, Keio University, Tokyo, Japan.

iso-TEtraQuinoline (*i*-TEQ): an inherently chiral N4 macrocyclic quinoline tetramer

Cyclic concatenation of four quinoline units affords a fully sp^2-hybridized, non-planar macrocycle featuring four inwardly oriented, coordinatively active pyridyl nitrogen atoms. The previously reported tetramer TEtraQuinoline (**TEQ**) exhibits head-to-tail connectivity of its quinoline units, affording an achiral architecture possessing S_4 symmetry. Herein, we report the design and synthesis of *iso*-TEtraQuinoline (***i*-TEQ**), an inherently chiral analogue featuring head-to-head connectivity at the 2,2'- and 8,8'-positions, which gives rise to a D_2-symmetric architecture. Detailed comparative investigations of the connectivity isomers ***i*-TEQ** and **TEQ** revealed an array of distinct characteristics.

Image reproduced by permission of Naoya Kumagai from *Chem. Sci.*, 2025, **16**, 10714.

As featured in:

See Naoya Kumagai *et al.*, *Chem. Sci.*, 2025, **16**, 10714.

ROYAL SOCIETY OF **CHEMISTRY**

15 YEARS ANNIVERSARY

rsc.li/chemical-science

ROYAL SOCIETY OF CHEMISTRY

EDGE ARTICLE

Check for updates

All publication charges for this article have been paid for by the Royal Society of Chemistry

iso-TEtraQuinoline (*i*-TEQ): an inherently chiral N4 macrocyclic quinoline tetramer†

Ryota Yagami,‡[a] Wei Xu, [ID] ‡[a] Toi Kobayashi, [ID] [a] Yuuya Nagata [ID] [b] and Naoya Kumagai [ID] *[ac]

Chiral macrocycles are attracting growing interest due to their broad applicability as ligands in asymmetric catalysis and as host molecules for chiral recognition. Robustness and high thermodynamic stability can be effectively achieved by strategically linking aromatic panels to construct an axially chiral macrocyclic framework. Cyclic concatenation of four quinoline units affords a fully sp²-hybridized, non-planar macrocycle featuring four inwardly oriented, coordinatively active pyridyl nitrogen atoms. The previously reported tetramer TEtraQuinoline (**TEQ**) exhibits head-to-tail connectivity of its quinoline units, affording an achiral architecture possessing S_4 symmetry. Herein, we report the design and synthesis of *iso*-TEtraQuinoline (*i*-TEQ), an inherently chiral analogue featuring head-to-head connectivity at the 2,2′- and 8,8′-positions, which gives rise to a D_2-symmetric architecture. Detailed comparative investigations of the connectivity isomers *i*-TEQ and **TEQ** revealed an array of distinct characteristics, including the overall architecture, intrinsic macrocyclic strain, spatial orientation of nitrogen lone pairs, thermodynamic stability, racemisation behaviour, metal complex stability, and circularly polarised luminescence.

Introduction

The chemical space occupied by axially chiral entities has remarkably expanded over the past several decades owing to their diverse applications as chiral ligands,[1] chiral sensing materials,[2] and biologically active natural or artificial products.[3] Due to their high thermodynamic stability and structural robustness, axially chiral molecules composed of sp²-hybridized aromatic units have attracted considerable attention for the construction of well-defined chiral environments in catalysis and sensing applications. The 1,1′-binaphthyl unit represents a privileged scaffold for this purpose and is extensively utilized in catalyst design by incorporating chalcogen and pnictogen atoms at 2,2′-positions to promote enantioselective metal- and organocatalysis, and molecular recognition[4] (Fig. 1a). In contrast, the 8,8′-biquinoline framework, which is structurally analogous to the 1,1′-binaphthyl but features an N(sp²) atom in place of one C(sp²)–H unit, is utilized only sparingly due to its relatively low racemisation barrier[5] (Fig. 1b). Incorporating the
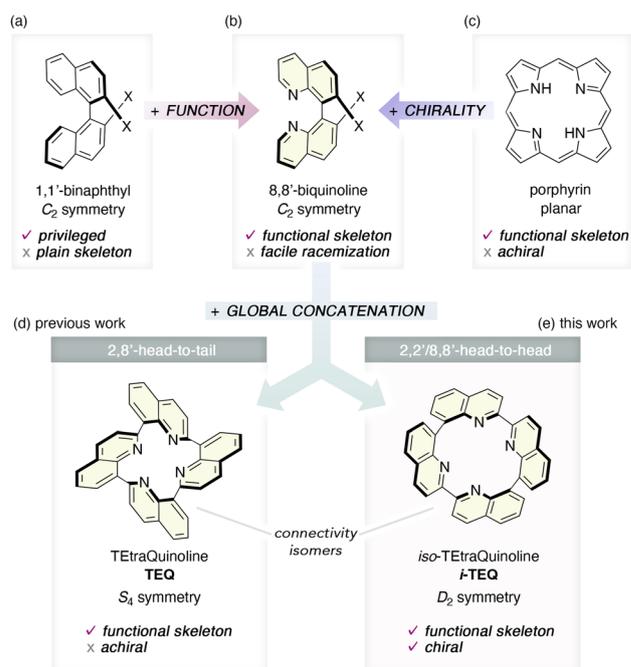

Fig. 1 Hierarchical structural modulation with respect to axial chirality and intrinsic functionality. (a–c) Structure and properties of 1,1′-binaphthyl, 8,8′-biquinoline, and porphyrin. (d) Previously studied TEtraQuinoline (**TEQ**) and its architectural features. (e) The newly developed macrocyclic quinoline framework, *iso*-TEtraQuinoline (*i*-TEQ), embodies both intrinsic functionality and inherent chirality.

[a]Graduate School of Pharmaceutical Sciences, Keio University, 1-5-30 Shibakoen, Minato-ku, Tokyo 105-8512, Japan. E-mail: kumagai-ny@keio.jp

[b]Institute for Chemical Reaction Design and Discovery (WPI-ICReDD), Hokkaido University, Hokkaido Kita 21, Nishi 10, Kita-ku, Sapporo, Hokkaido 001-0021, Japan

[c]Institute of Microbial Chemistry, 3-14-23 Kamiosaki, Shinagawa-ku, Tokyo 141-0021, Japan

† Electronic supplementary information (ESI) available. CCDC 2392427, 2392429, 2392433, 2392428 and 2392430. For ESI and crystallographic data in CIF or other electronic format see DOI: https://doi.org/10.1039/d5sc02937f

‡ These authors contributed equally.

quinoline unit is particularly advantageous, as it not only imparts axially chirality but also introduces a functional motif capable of coordinating metal cations, thereby offering dual functionality in a single framework. Inspired by porphyrin— a representative functional framework ubiquitous in nature that coordinates metal cations through four sp²-hybridized nitrogen atoms—we previously designed a tetrameric quinoline construct, TEtraQuinoline (**TEQ**), as a non-planar analogue of porphyrin.[6] While its cyclic concatenation effectively suppresses the flipping of the linked quinoline units, the head-to-tail assembly through the 2- and 8-positions imparts an overall achiral, S_4-symmetric rigid architecture to the **TEQ** framework. Given the diverse chemistry exhibited by **TEQ** in metal coordination, photophysical behaviour, and catalytic applications,[7] the development of its chiral variant is highly desirable. Herein, we report the re-design of a quinoline-based, axially chiral molecular framework that functions as a tetradentate nitrogen ligand: iso-TEtraQuinoline (**i-TEQ**).[8] By switching the ring connectivity from head-to-tail to head-to-head at the 2,2'- and 8,8'-positions, **i-TEQ** adopts a D_2-symmetric, inherently chiral architecture.[9] Detailed comparative structural analyses uncovered similarities and differences between these connectivity isomers, highlighting the impact of the concatenation pattern on the chemical and photophysical properties.

Results and discussion
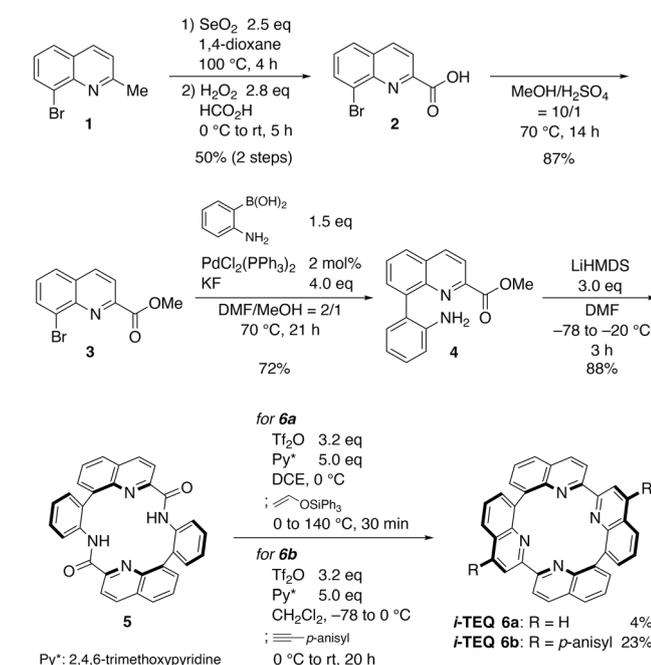
Synthesis of iso-TEtraQuinolines (i-TEQs)

Inspired by the **TEQ** framework, we designed a synthetic plan utilizing cyclic diamide **5** with two quinoline units as a key precursor to **i-TEQ** via a two-fold quinoline forming reaction (Scheme 1). The synthesis of **i-TEQ** was initiated by a two-step

benzylic oxidation of 8-bromo-2-methylquinoline **1** mediated by SeO₂ and H₂O₂/HCO₂H to afford carboxylic acid **2**. After converting **2** into methyl ester **3** with H₂SO₄ in MeOH, Suzuki–Miyaura cross-coupling with (2-amino)phenylboronic acid afforded aminoester **4**.[10] Following brief screening,[11] simple cryogenic and highly diluted conditions with LiHMDS engaged **4** in smooth amidative dimerization, furnishing the requisite cyclic diamide **5** in 88% yield. According to Movassaghi's protocol[12] and our previous modification for quinoline formation from macrocyclic amides,[6a,h,i] electrophilic activation of the amide functionality using Tf₂O and 2,4,6-trimethoxypyridine and subsequent formal cycloaddition afforded the **i-TEQ** architecture. Quinoline formation with (triphenylsiloxy)ethylene furnished non-substituted D_2-symmetric **i-TEQ 6a**, but the yield was only 4%. More reactive p-anisylacetylene allowed for a more efficient ring reinforcement reaction to give C_2-symmetric bis-p-anisylated **i-TEQ 6b** in 23% yield. The p-anisyl groups of **i-TEQ 6b** can be smoothly demethylated, enabling further structural elaboration.[13]

A detailed comparative structural analysis was performed on the thus-obtained **i-TEQ 6b**—a connectivity isomer of p-anisylated **TEQ 7b** sharing the same atomic composition (Fig. 2). To minimize structural deviations caused by crystal packing effects, DFT-optimized structures of both isomers were compared using the B3LYP-D3/6-31G(d,p) level of theory with the IEFPCM(CHCl₃) solvation model (Fig. 2a).[14] Comparison of the top views of these structures revealed a distinct difference in the inner hollow topology: **i-TEQ 6b** features a diamond-shaped 16-membered macrocycle, while **TEQ 7b** exhibits a square-like counterpart. In contrast, the spatial arrangement of the four nitrogen atoms is similar, with the distances between diagonal nitrogen atoms being nearly identical, ranging from 4.35 to 4.47 Å. Additionally, the τ'_4 values[15] are close to zero, suggesting that **i-TEQ 6b**, like **TEQ 7b**, is capable of accommodating metal cations that prefer a square planar coordination mode (Fig. 2a and b). The diamond-shaped cavity of **i-TEQ 6b** arises from the head-to-head (2,2' and 8,8') linkage of the quinoline units, leading to an overall laterally distorted structure characterized by reduced dihedral angles and an increased vertical dimension (**i-TEQ 6b**: 6.56 Å vs. **TEQ 7b**: 6.01 Å). Whereas the D_2-symmetric **i-TEQ** skeleton is more stable than the S_4-symmetric **TEQ** skeleton (ΔG = 2.2 kcal mol⁻¹), enthalpic evaluation via a homodesmotic reaction[16] and StrainViz analysis[17] indicated that **i-TEQ** adopts a more strained architecture (difference in total strain: 9.0 kcal mol⁻¹), with the local structures of the intrinsic quinoline units being more distorted (Fig. 2b–d). This seemingly contradictory outcome is attributed to electronic repulsion between the lone pairs on the inwardly oriented nitrogen atoms; those of **i-TEQ** are oriented in a mutually more skewed fashion to prevent undesired overlapping. This electronic factor likely outweighs the skeletal distortion, rendering **i-TEQ** more thermodynamically stable than **TEQ**, as supported by TG-DTA analysis; **i-TEQ 6b** remains stable above 300 °C, whereas **TEQ 7b** begins to decompose above 250 °C.[18]

Physicochemical properties of i-TEQs

The structural rigidity of the **i-TEQ** framework, a cyclic assembly of four quinoline panels with a hitherto unknown pattern of

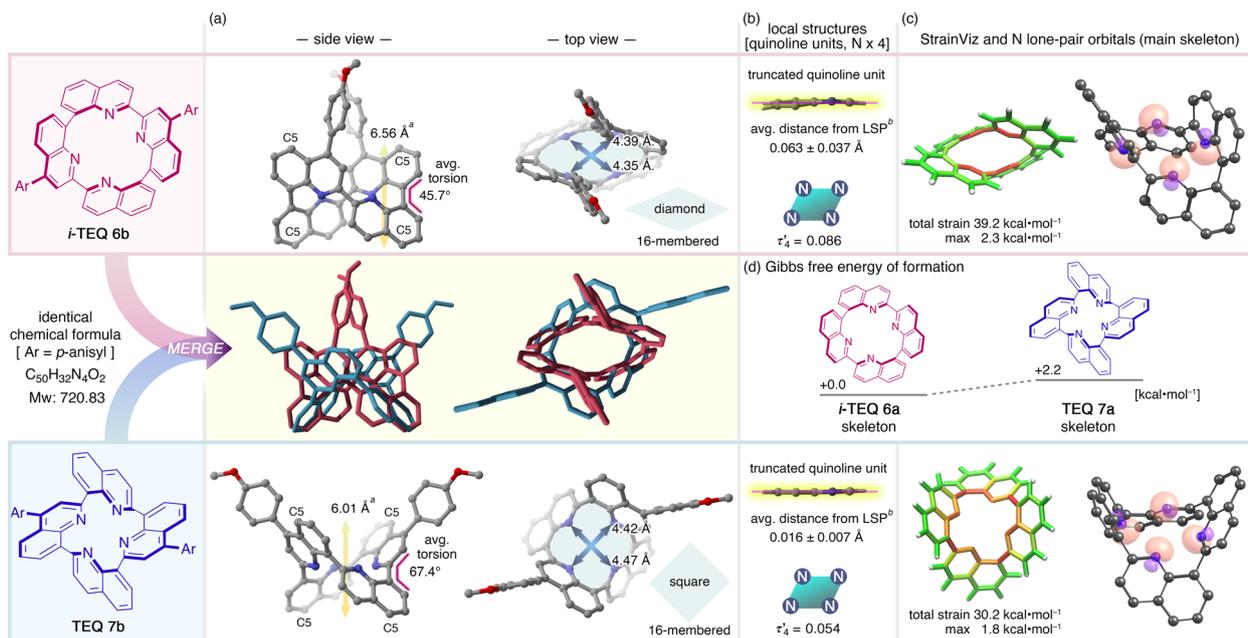**Scheme 1** Synthesis of i-TEQ **6a**, **6b**.

Fig. 2 Structural comparison of connectivity isomers *i*-TEQ 6b and TEQ 7b sharing a tetrameric quinoline macrocyclic architecture and two peripheral diagonal *p*-anisyl groups. (a) Optimized structures are calculated at the B3LYP-D3/6-31G(d,p)/IEFPCM(CHCl$_3$) level of theory. Colour codes; carbon: grey, nitrogen: blue, oxygen: red, hydrogen atoms are omitted for clarity. [a]Vertical size of the main framework is calculated by the distance between the midpoint of the two quinoline C5 carbons on the upper side and the midpoint of the two quinoline C5 carbons on the lower side. (b) Analysis of local structures. [b]LSP: least squares plane. More detailed analysis is summarized in ESI.† (c) StrainViz analysis and NBO of nitrogen lone pairs. StrainViz calculation was carried out at the B3LYP/6-31G(d) level of theory. (d) Comparison of Gibbs free energy for the formation of non-substituted *i*-TEQ 6a and TEQ 7a.

connectivity, is great of interest. Racemic samples of D_2-symmetric non-substituted *i*-TEQ 6a and C_2-symmetric *p*-anisylated *i*-TEQ 6b were optically resolved *via* preparative HPLC on a chiral stationary phase (Fig. 3a). 6a and 6b were successfully resolved with base-peak separation under identical conditions (DAICEL CHIRALPAK IB-N5, ^{n}hexane/CH$_2$Cl$_2$ mixed solvent

Fig. 3 (a) Partial HPLC chromatogram for optical resolution of *rac-i*-TEQ 6a and 6b separated by DAICEL CHIRALPAK IB-N5 column with ^{n}hexane/CH$_2$Cl$_2$ eluent. (b) Circular dichroism (CD) spectra of optically pure samples of non-substituted (+)- and (−)-*i*-TEQ 6a, and anisylated (+)- and (−)-*i*-TEQ 6b in CH$_2$Cl$_2$ (25 μM).

eluent). The initially eluted enantiomers of both 6a and 6b displayed a positive Cotton effect in a range of 330–350 nm, corresponding to HOMO–LUMO excitation (Fig. 3b).[19] DFT simulations of electronic CD spectra suggested the absolute configuration shown in Fig. 3a.[20] Intriguingly, optical rotation of the first eluents of 6a and 6b were opposite (6a: dextrorotatory, 6b: levorotatory), presumably because the closely located diagonal *p*-anisyl groups of 6b affected optical rotation at the wavelength of sodium D-lines.

The stereochemical integrity of (−)-*i*-TEQ 6b was traced at a 1 mg mL^{-1} concentration in diphenyl ether under various conditions (Table 1). The initial racemisation attempt without any additive confirmed that the stereochemistry of the *i*-TEQ architecture is quite stable; no decomposition or erosion of enantiopurity was observed even at 220 °C for 24 h (Entry 1). DFT calculations on the non-substituted *i*-TEQ 6a successfully reproduced the experimentally observed high racemisation barrier, yielding an inversion barrier of 58.0 kcal mol^{-1} for the transition state at the B3LYP-D3/6-311+G(2d,p)/SMD(diethyl ether) level of theory (Fig. 4a). Given that structurally similar acyclic azaBINOL is readily racemised (28.4 kcal mol^{-1}),[5a] the unusual retention of axial chirality of *i*-TEQ is likely due to its unique concatenated structure. Notably, the inversion barrier of *i*-TEQ 6a is even higher than that of the configurationally stable TEQ 7a (56.9 kcal mol^{-1} at the B3LYP-D3/6-31G(d,p) level of theory), and the inversion process proceeds *via* a stepwise mechanism involving a C_i-symmetric intermediate, in contrast to the single-step flipping observed for TEQ 7a (Fig. 4a). We
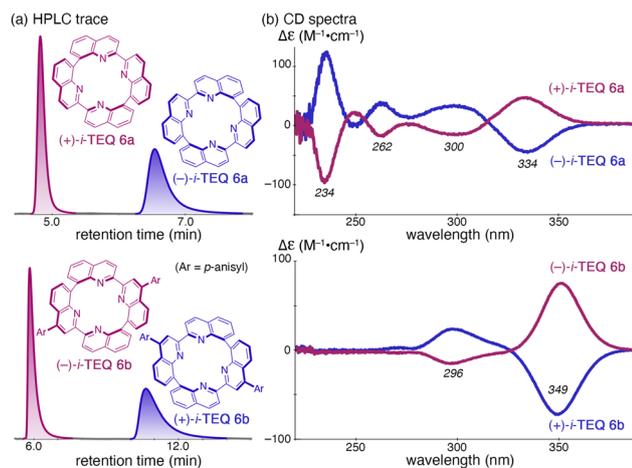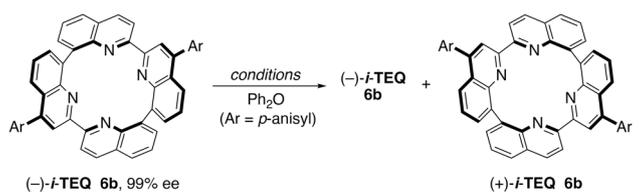
Table 1 Racemisation study of *i*-TEQ 6b in the absence or presence of additives

Entry	Additive[a]	Temp. (°C)	Time (h)	ee[b] (%)	Rate constant ($\times 10^{-7}$ s^{-1})	$t_{1/2}$ (h)	$\Delta G_{exp}^{\ddagger}$ (kcal·mol^{-1})	$\Delta G_{calc}^{\ddagger}$ [c] (kcal·mol^{-1})
1	None	220	24	>99	—[d]	—	—	58.0
2	TFA	140	24	>99	—[d]	—	—	50.8[e], 46.3[f]
3		160	56	91	2.18	883	38.9	
4	[Pd(MeCN)$_4$](BF$_4$)$_2$	100	30	63	20.2	95.3	31.8	33.3
5		140	2.5	20	888	2.2	32.1	
6	CoCl$_2$	100	24	>99	—[d]	—	—	30.6
7		140	56	88	2.99	644	36.8	
8	CuCl$_2$	100	24	>99	—[d]	—	—	34.4
9		140	30	72	14.8	130	35.5	

[a] 1 Equivalent of additives was added. [b] Determined by chiral stationary phase HPLC analysis. [c] $\Delta G_{calc}^{\ddagger}$ was calculated on non-substituted *i*-TEQ 6a at the B3LYP-D3/6-311+G(2d,p)-SDD(Co,Cu,Pd)/SMD(diethyl ether) level of theory. Compared with Fig. 4, a more extended basis set was employed and an appropriate solvation model was applied. [d] No racemisation occurred. [e] Calculated on the monoprotonated model. [f] Calculated on the diprotonated model.

reasoned that mitigating the repulsive orbital interactions of the four inwardly oriented nitrogen atoms enhanced the racemisation. While racemisation of (−)-*i*-TEQ 6b barely proceeded in the presence of 1 equivalent of trifluoroacetic acid (TFA) at 140 °C, a higher temperature (160 °C) induced slow the racemisation ($t_{1/2}$ = *ca.* 37 days) (Table 1, Entries 2,3). Quinoline ring flipping was significantly accelerated by the addition of [Pd(MeCN)$_4$](BF$_4$)$_2$ with $t_{1/2}$ of 2.2 h at 140 °C (20% ee after 2.5 h), which corresponds to an empirically determined flipping

barrier of 32.1 kcal mol^{-1} (Entries 4,5). Intriguingly, *p*-anisylated (−)-TEQ 7b, featuring head-to-tail concatenation, was significantly more reluctant to racemise and remained at 88% ee even after 24 h of stirring under identical conditions (with Pd salt at 140 °C).[21] This distinct response to the Pd^{2+} cation was reproduced by DFT calculations (Fig. 4b); the pathway from the *i*-TEQ 6a/Pd^{2+} complex to its antipode involves a series of local minima connected by partially flipped C_1- and C_s-symmetric transition states, which significantly lower the inversion barrier.
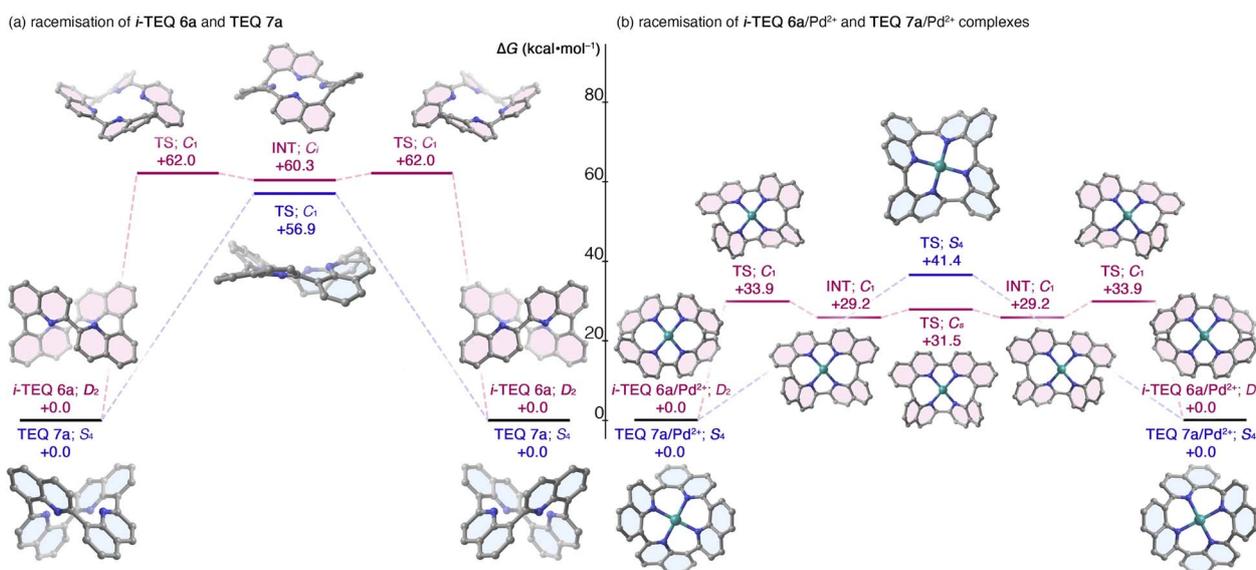

Fig. 4 Stereoinversion of non-substituted quinoline tetramers in the absence and presence of Pd^{2+} cation. Calculated at the B3LYP-D3/6-31G(d,p)-SDD(Pd) level of theory. (a) *i*-TEQ 6a and TEQ 7a, and (b) *i*-TEQ 6a/Pd^{2+} complex and TEQ 7a/Pd^{2+} complexes.
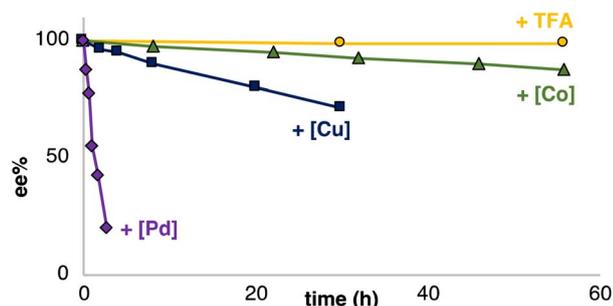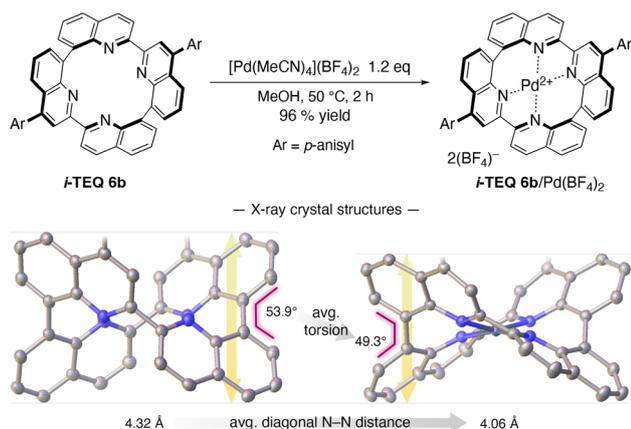
Fig. 5 Racemisation profile of enantiopure (−)-*i*-TEQ **6b** in the presence of additives (1 eq) at 140 °C in diphenyl ether (1 mg mL^{-1}). A plot of enantiomeric excess (%) *versus* time is shown. Enantiomeric excess was determined by chiral stationary phase HPLC analysis.

In contrast, the **TEQ 7a**/Pd^{2+} complex undergoes a high-energy S_4-symmetric transition state to achieve stereoinversion. Other azophilic metal cations featuring a square planar coordination mode, *e.g.* Co^{2+} or Cu^{2+} rendered racemisation, whereas acceleration was significantly smaller than that of Pd^{2+} and no racemization occurred at a temperature not exceeding 100 °C (Table 1, Entries 6–9). A plot of enantiomeric excess and elapsed time clearly demonstrates the substantial rigidity and characteristic response to Pd^{2+} in the racemisation of (−)-*i*-TEQ **6b** (Fig. 5). DFT calculations located energetically more favourable transition states by protonation or metal coordination.[22]
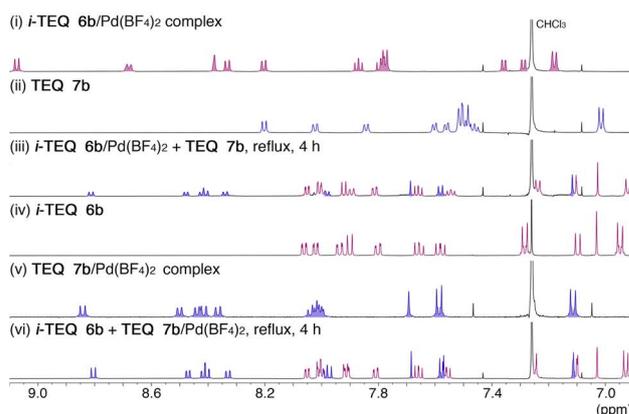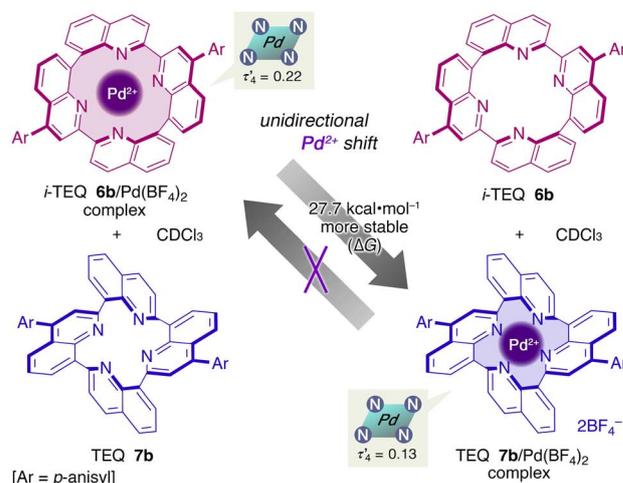
The accelerated racemisation of (−)-*i*-TEQ **6b** in the presence of Pd^{2+} demonstrates that *i*-TEQ is capable of accommodating Pd^{2+} cations despite the highly twisted configuration of the lone pair orbitals of the four quinoline nitrogen atoms (Fig. 2c). Indeed, treatment of *i*-TEQ **6b** with [Pd(MeCN)$_4$][(BF$_4$)$_2$] in MeOH at 50 °C furnished the *i*-TEQ **6b**/Pd(BF$_4$)$_2$ complex in excellent yield (Scheme 2). Comparative X-ray diffraction analysis of the crystal structures of *i*-TEQ **6b** and *i*-TEQ **6b**/Pd(BF$_4$)$_2$ revealed that both the averaged torsion angle at 8,8′-biquinoline units and the averaged distance of the diagonal nitrogen atoms

decreased upon complexation from 53.9° to 49.3° and from 4.32 to 4.06 Å, respectively, leading to a vertically collapsed architecture.

To probe the thermodynamic stability of the Pd^{2+} complexes of *i*-TEQ **6b** and **TEQ 7b**, structural isomers with an identical elemental composition, a ligand metathesis experiment was conducted (Scheme 3). The *i*-TEQ **6b**/Pd(BF$_4$)$_2$ complex and metal-free **TEQ 7b** were mixed in CDCl$_3$ and heated under reflux. ^{1}H NMR revealed that the signals derived from both the *i*-TEQ **6b**/Pd(BF$_4$)$_2$ complex and the **TEQ 7b** completely disappeared (Scheme 3, (i,ii) *vs.* (iii)). Instead, newly observed peaks corresponded to the free forms of *i*-TEQ **6b** and the **TEQ 7b**/Pd(BF$_4$)$_2$ complex (Scheme 3, (iii) *vs.* (iv, v)). In contrast, under identical conditions, a mixture of the free form of *i*-TEQ **6b** with the **TEQ 7b**/Pd(BF$_4$)$_2$ complex displayed virtually no change in ^{1}H NMR analysis, confirming the unidirectional Pd^{2+} cation swapping from *i*-TEQ **6b** to **TEQ 7b** (Scheme 3 (iv,v) *vs.* (vi)). The empirically observed higher stability of the Pd^{2+} complex of **TEQ 7b** over that of *i*-TEQ **6b** was reproduced by DFT calculations at the B3LYP-D3/6-31G(d,p)-SDD(Pd)/

Scheme 2 Complexation of *i*-TEQ **6b** with [Pd(MeCN$_4$)](BF$_4$)$_2$, and crystal structures of the **6b** and **6b**/Pd(BF$_4$)$_2$ complex. ORTEP drawings are shown at 50% probability ellipsoids. Colour codes; carbon: grey, nitrogen: blue, oxygen: red, palladium: dark blue. Hydrogen atoms, *p*-anisyl substituents, and counter anions were omitted for clarity.

Scheme 3 Unidirectional Pd^{2+} cation swapping between *i*-TEQ **6b** and **TEQ 7b**. Partial ^{1}H NMR spectra in CDCl$_3$ (i) *i*-TEQ **6b**/Pd(BF$_4$)$_2$; (ii) **TEQ 7b**; (iii) *i*-TEQ **6b**/Pd(BF$_4$)$_2$ + **TEQ 7b** at reflux temperature after 4 h; (iv) *i*-TEQ **6b**; (v) **TEQ 7b**/Pd(BF$_4$)$_2$; (vi) **TEQ 7b**/Pd(BF$_4$)$_2$ + *i*-TEQ **6b** at reflux temperature after 4 h.
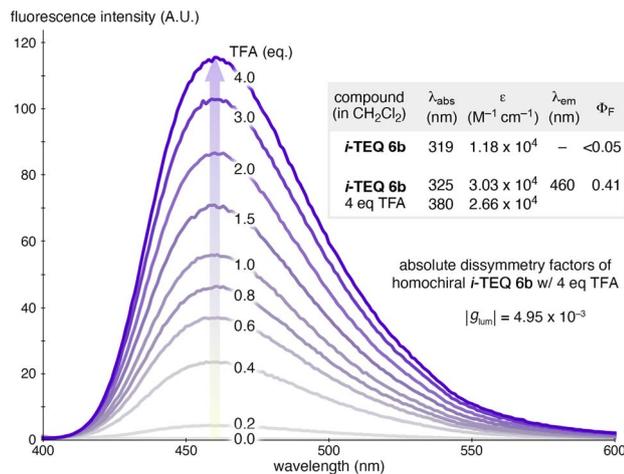
Fig. 6 Photophysical properties of *i*-TEQ **6b**. Fluorescence spectra of *i*-TEQ **6b** in CH_2Cl_2 (20 μM) were recorded upon incremental addition of TFA in CH_2Cl_2 (excitation at 385.5 nm).

IEFPCM($CHCl_3$) level of theory; [*i*-TEQ **6b** + **TEQ 7b**/Pd^{2+}] is 27.7 kcal mol^{-1} more stable than [*i*-TEQ **6b**/Pd^{2+} + **TEQ 7b**].

The photophysical properties of *i*-TEQ **6b** were systematically investigated. Although *i*-TEQ **6b** is inherently barely emissive, the addition of TFA induced a pronounced fluorescence enhancement in an equivalence-dependent manner (Fig. 6). In CH_2Cl_2, the fluorescence intensity of *i*-TEQ **6b** increased progressively with the incremental addition of TFA, reaching a plateau at 4 equivalents (460 nm, $\Phi_F = 0.41$). This acid-responsive fluorescence behaviour, combined with the inherent chirality of **6b**, prompted us to explore its potential in circularly polarized luminescence (CPL). Enantiomerically pure samples of (+)-**6b** and (−)-**6b** exhibited mirror-image CPL spectra upon the addition of 4 equivalents of TFA, with an absolute luminescence dissymmetry factor ($|g_{lum}|$) of 4.95×10^{-3}.[23] Notably, this value is an order of magnitude greater than that of ring-connectivity isomer **TEQ 7b**,[6a] highlighting the strong influence of the concatenation pattern on the resultant physicochemical properties.[24]

Derivatization from cyclic diamide

Cyclic diamide **5**, a key intermediate in the synthesis of *i*-TEQs, serves as a flexible N4 macrocyclic scaffold (Scheme 4). Partial reduction of the amide moiety of **5** using the Zr-based Schwartz reagent[25] afforded diimine **8** in 54% yield. Reduction to secondary amines was achieved *via* Ir-catalysed silane conditions,[26] affording tetradentate ligand **9**. While electrophilic activation of the amide with Tf_2O followed by formal cycloaddition with alkynes furnishes the quinoline ring en route to *i*-TEQs (*vide supra*), a two-fold intramolecular cyclization by the neighbouring quinoline proceeded in the absence of an external nucleophile to afford a warped, tetraaza dicationic π-material **10**. A brief base screening identified electron-deficient 2-chloropyridine as optimal, providing **10** in 79% yield. **10** was readily reduced to furnish a more stable, neutral fused polycyclic material **11**,[27] whose unique three-dimensional structure was unambiguously determined by X-ray crystallographic analysis.
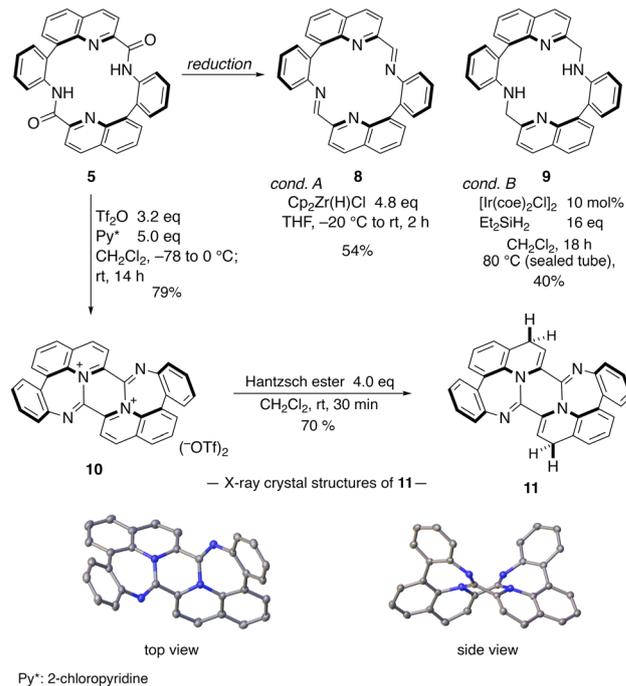
Scheme 4 Derivatization from cyclic diamide **5**.

Conclusions

Here, we describe the design and synthesis of a D_2-symmetric *iso*-TEtraQuinoline (*i*-TEQ) as an inherently, three-dimensional analogue of porphyrin. *i*-TEQ is a head-to-head quinoline tetramer and a connectivity isomer of previously reported S_4-symmetric, achiral **TEQ**, in which four quinoline units are concatenated in a head-to-tail fashion. Comprehensive and systematic comparable analyses of *i*-TEQ and **TEQ** revealed the unique features of these closely related molecular entities in terms of their overall architecture, stereochemical integrity, intrinsic ring strain, metal complexation abilities, and photophysical behaviour. Given its built-in chirality, *i*-TEQ represents a unique molecular scaffold that will serve as a cornerstone in the development of chiral porphyrinoids, thereby expanding the chemical space of porphyrin-based materials.

Data availability

Experimental and characterization data, including crystallographic data [**5** (CCDC 2392427), **6b** (CCDC 2392429), and **6d** (CCDC 2392433), **6b**/Pd(BF_4)$_2$ (CCDC 2392430), **11** (CCDC 2392428)], photophysical measurements, and NMR spectra, as well as computational investigations. The data supporting this article have been included as part of the ESI.†

Author contributions

N. K. and W. X. conceived and directed the project. R. Y. and W. X. synthesised, analysed, and characterised all compounds. T. K. performed theoretical calculations with partial support

Conflicts of interest

There are no conflicts to declare.

Acknowledgements

Notes and references

1 (a) Y.-B. Wang and B. Tan, *Acc. Chem. Res.*, 2018, **51**, 534–547; (b) J. K. Cheng, S.-H. Xiang, S. Li, L. Ye and B. Tan, *Chem. Rev.*, 2021, **121**, 4805–4902; (c) G.-J. Mei, W. L. Koay, C.-Y. Guan and Y. Lu, *Chem*, 2022, **8**, 1855–1893.

2 (a) L. Pu, *Chem. Rev.*, 1998, **98**, 2405–2494; (b) L. Pu, *Acc. Chem. Res.*, 2012, **45**, 150–163.

3 (a) G. Bringmann, T. Gulder, T. A. M. Gulder and M. Breuning, *Chem. Rev.*, 2011, **111**, 563–639; (b) S. R. LaPlante, L. D. Fader, K. R. Fandrick, D. R. Fandrick, O. Hucke, R. Kemper, S. P. F. Miller and P. J. Edwards, *J. Med. Chem.*, 2011, **54**, 7005–7022; (c) M. Basilaia, M. H. Chen, J. Secka and J. L. Gustafson, *Acc. Chem. Res.*, 2022, **55**, 2904–2919; (d) B. A. Lanman, A. T. Parsons and S. G. Zech, *Acc. Chem. Res.*, 2022, **55**, 2892–2903; (e) Z. Wang, L. Meng, X. Liu, L. Zhang, Z. Yu and G. Wu, *Eur. J. Med. Chem.*, 2022, **243**, 114700.

4 For selected reviews on asymmetric catalysis with 1,1'-bi-2-naphthol (BINOL); (a) Y. Chen, S. Yekta and A. K. Yudin, *Chem. Rev.*, 2003, **103**, 3155–3212; (b) L. Eberhardt, D. Armspach, J. Harrowfield and D. Matta, *Chem. Soc. Rev.*, 2008, **37**, 839–864; (c) P. W. N. M. van Leeuwen, P. C. J. Kamer, C. Claver, O. Pàmies and M. Diéguez, *Chem. Rev.*, 2011, **111**, 2077–2118; (d) D. Parmar, E. Sugiono, S. Raja and M. Rueping, *Chem. Rev.*, 2014, **114**, 9047–9153; (e) L. Pu, *Chem. Rev.*, 2024, **124**, 6643–6689. For lanthanum–lithium–BINOL (LLB) complexes; (f) M. Shibasaki and N. Yoshikawa, *Chem. Rev.*, 2002, **102**, 2187–2210; (g) N. Kumagai, M. Kanai and H. Sasai, *ACS*

Catal., 2016, **6**, 4699–4709. For the other phosphines, amides, and others; (h) Q.-H. Fan, Y.-M. Li and A. S. C. Chan, *Chem. Rev.*, 2002, **102**, 3385–3466; (i) M. Berthod, G. Mignani, G. Woodward and M. Lemaire, *Chem. Rev.*, 2005, **105**, 1801–1836; (j) T. Akiyama and K. Mori, *Chem. Rev.*, 2015, **115**, 9277–9306; (k) H. Ni, W.-L. Chan and Y. Lu, *Chem. Rev.*, 2018, **118**, 9344–9411; For 1,1'-binaphthyl-based macrocycles; (l) R. Ning, H. Zhou, S.-X. Nie, Y.-F. Ao, D.-X. Wang and Q.-Q. Wang, *Angew. Chem., Int. Ed.*, 2020, **59**, 10894–10898; (m) G. Sun, X. Zhang, Z. Zheng, Z.-Y. Zhang, M. Dong, J. L. Sessler and C. Li, *J. Am. Chem. Soc.*, 2024, **146**, 26233–26242.

5 (a) P. R. Blakemore, C. Kilner and S. D. Milicevic, *J. Org. Chem.*, 2006, **71**, 8212–8218; (b) J. Xiao and T.-P. Loh, *Org. Lett.*, 2009, **11**, 2876–2879; (c) S.-M. Sephton, C. Wang, L. N. Zakharov and P. R. Blakemore, *Eur. J. Org Chem.*, 2012, 3249–3260; (d) J. V. Chocholoušová, J. Vacek, A. Andronova, J. Míšek, O. Songis, M. Šámal, I. G. Stará, M. Meyer, M. Bourdillon, L. Pospíšil and I. Starý, *Chem.–Eur. J.*, 2014, **20**, 877–893.

6 (a) W. Xu, Y. Nagata and N. Kumagai, *J. Am. Chem. Soc.*, 2023, **145**, 2609–2618. Other examples of quinoline-based macrocycles; (b) P. S. Shirude, E. R. Gillies, S. Ladame, F. Godde, K. Shin-ya, I. Huc and S. Balasubramanian, *J. Am. Chem. Soc.*, 2007, **129**, 11890–11891; (c) T. Shimasaki, R. Kuroda, M. Akao, T. Akimoto, T. Ishikawa, T. Iwanaga, N. Teramoto and M. Shibata, *Chem. Lett.*, 2019, **48**, 133–136; (d) S. Adachi, M. Shibasaki and N. Kumagai, *Nat. Commun.*, 2019, **10**, 3820; (e) D. Yang, J. L. Greenfield, T. K. Ronson, L. K. S. von Krbek, L. Yu and J. R. Nitschke, *J. Am. Chem. Soc.*, 2020, **142**, 19856–19861; (f) T. Kobayashi and N. Kumagai, *Angew. Chem., Int. Ed.*, 2023, **62**, e202307896; (g) T. Kobayashi, T. Sakurai and N. Kumagai, *Bull. Chem. Soc. Jpn.*, 2023, **96**, 1139–1143; (h) K. Kihara, T. Kobayashi, W. Xu and N. Kumagai, *Chem.–Eur. J.*, 2024, **30**, e202304176; (i) T. Karimata, W. Xu and N. Kumagai, *Chem.–Eur. J.*, 2025, **31**, e202404335.

7 M. Nishiwaki, W. Xu and N. Kumagai, *Asian J. Org. Chem.*, 2023, **12**, e202300261.

8 For the naphthalene analogue; (a) Y. Nojima, M. Hasegawa, N. Hara, Y. Imai and Y. Mazakia, *Chem. Commun.*, 2019, **55**, 2749–2752; (b) Y. Nojima, M. Hasegawa, N. Hara, Y. Imai and Y. Mazaki, *Chem.–Eur. J.*, 2021, **27**, 5923–5929.

9 For other inherently chiral macrocyclic compounds, see: (a) S. Tong, J.-T. Li, D.-D. Liang, Y.-E. Zhang, Q.-Y. Feng, X. Zhang, J. Zhu and M.-X. Wang, *J. Am. Chem. Soc.*, 2020, **142**, 14432–14436; (b) H. Han, X.-G. Wang, S. Tong, J. Zhu and M.-X. Wang, *ACS Catal.*, 2025, **15**, 6018–6024; (c) S. J. Nemat, H. Jędrzejewska, A. Prescimone, A. Szumna and K. Tiefenbacher, *Org. Lett.*, 2020, **22**, 5506–5510; (d) G. E. Arnott, *Chem.–Eur. J.*, 2018, **24**, 1744–1754; (e) F. Sannicolò, P. R. Mussini, T. Benincori, R. Cirilli, S. Abbate, S. Arnaboldi, S. Casolo, E. Castiglioni, G. Longhi, R. Martinazzo, M. Panigati, M. Pappini, E. Q. Procopio and S. Rizzo, *Chem.–Eur. J.*, 2014, **20**, 15298–15302.

10 A. Suzuki, *Angew. Chem., Int. Ed.*, 2011, **50**, 6722–6737.

11 See ESI Section 2.6† for details.

12 M. Movassaghi and M. D. Hill, *J. Am. Chem. Soc.*, 2006, **128**, 14254–14255.

13 See ESI Section 2.9 and 2.10† for details.

14 X-ray crystallographic analysis of *i*-**TEQ 6b** and **TEQ 7b** revealed that crystal structures and calculated structures of the main frameworks are almost identical.

15 A. Okuniewski, D. Rosiak, J. Chojnacki and B. Becker, *Polyhedron*, 2015, **90**, 47–57.

16 See ESI Section 7.7† for details.

17 C. E. Colwell, T. W. Price, T. Stauch and R. Jasti, *Chem. Sci.*, 2020, **11**, 3923–3930.

18 See ESI Fig. S28 and S29.†

19 See ESI Table S4† for details.

20 See ESI Fig. S17 and S18.†

21 See ESI Section 5.3† for details.

22 See ESI Section 6† for details.

23 G. Longhi, E. Castiglioni, J. Koshoubu, G. Mazzeo and S. Abbate, *Chirality*, 2016, **28**, 696–707. See ESI Section 7.5† for experimental details.

24 See ESI Section 7.6† for calculational details.

25 J. Schwartz and J. A. Labinger, *Angew. Chem., Int. Ed.*, 1976, **15**, 333–340.

26 C. Cheng and M. Brookhart, *J. Am. Chem. Soc.*, 2012, **134**, 11304–11307.

27 For fused polycyclic material see following reviews or latest articles; (*a*) H. Ito, K. Ozaki and K. Itami, *Angew. Chem., Int. Ed.*, 2017, **56**, 11144–11164; (*b*) S. H. Pun and Q. Miao, *Acc. Chem. Res.*, 2018, **51**, 1630–1642; (*c*) G. G. Miera, S. Matsubara, H. Kono, K. Murakami and K. Itami, *Chem. Sci.*, 2022, **13**, 1848–1868; (*d*) S. M. Elbert, O. T. A. Paine, T. Kirschbaum, M. P. Schuldt, L. Weber, F. Rominger and M. Mastalerz, *J. Am. Chem. Soc.*, 2024, **146**, 27324–27334. For aza-substituted warped nano-sheets; (*e*) S. Ito, Y. Tokimaru and K. Nozaki, *Angew. Chem., Int. Ed.*, 2015, **54**, 7256–7260; (*f*) H. Yokoi, Y. Hiraoka, S. Hiroto, D. Sakamaki, S. Seki and H. Shinokubo, *Nat. Commun.*, 2015, **6**, 8215; (*g*) S. Higashibayashi, P. Pandit, R. Haruki, S. Adachi and R. Kumai, *Angew. Chem., Int. Ed.*, 2016, **55**, 10830–10834; (*h*) K. Oki, M. Takase, S. Mori, A. Shiotari, Y. Sugimoto, K. Ohara, T. Okujima and H. Uno, *J. Am. Chem. Soc.*, 2018, **140**, 10430–10434; (*i*) T. Kirschbaum, F. Rominger and M. Mastalerz, *Chem.–Eur. J.*, 2020, **26**, 14560–14564; (*j*) P. An, R. Li, B. Ma, R.-Y. He, Y.-K. Zhang, M.-J. Xiao and B. Zhang, *Angew. Chem., Int. Ed.*, 2021, **60**, 24478–24483; (*k*) J. Wagner, P. Z. Crocomo, M. A. Kochman, A. Kubas, P. Data and M. Lindner, *Angew. Chem., Int. Ed.*, 2022, **61**, e202202232; (*l*) M. Krzeszewski, Ł. Dobrzycki, A. L. Sobolewski, M. K. Cyrański and D. T. Gryko, *Chem. Sci.*, 2023, **14**, 2353–2360.